Differential lipid binding of vinculin isoforms promotes quasi-equivalent dimerization

Krishna Chinthalapudi[a,b], Erumbi S. Rangarajan[a,b], David T. Brown[c], and Tina Izard[a,b,1]

Cell Adhesion Laboratory,

[a]Department of Cancer Biology, The Scripps Research Institute, Jupiter FL 33458, USA

[b]Department of Immunology and Microbial Sciences, The Scripps Research Institute, Jupiter FL 33458, USA

[c]Department of Biochemistry, University of Mississippi Medical Center, Jackson, MS 39216

[1]To whom correspondence should be addressed:

E-mail: cmorrow@scripps.edu

MATERIALS AND METHODS

DNA Constructs

MVt wild type constructs (residues 959-1134 and 959-1130) were cloned into a modified pET-28a vector (EMD Millipore) with an *N*-terminal octa-histidine tag followed by a PreScission protease cleavage site. The MV quadruple mutant (R975Q, K979Q, R1107Q, R1128Q), the triple mutant (Q971R, R975D, T978R), and the vinculin triple mutant (R903Q, D907R, R910T) were generated by site-directed mutagenesis from the wild type MVt or Vt by using the Agilent Technology's QuickChange site-directed mutagenesis kit. The FRET probes were cloned into a modified pET15b vector with an *N*-terminal hexa-histidine tag followed by CFP and YFP in frame with MVt constructs (959-1134, Δ1131-4, R975W, and the quadruple mutant). The details of cloning, expression and purification of human full-length vinculin, human full-length MV and R975W mutant were described earlier (1). Human MV-encoding cDNA was fused in frame to the EGFP in a modified pCDNA4 vector with *N*-terminal His_{10} tag. The QuikChange® site-directed mutagenesis kit (Agilent Technologies) was used to generate EGFP tagged MV mutants Δ1131-4 and R975W. All mutants were sequenced and verified.

Protein Preparation

Expression plasmids were transformed in *Escherichia coli* strain BL21-DE3 (Invitrogen) or in BL21-CodonPlus (DE3)-RIL cells (Agilent Technology). For purification of MVt wild type, Δ1131-4, quadruple mutant, R975W, and triple mutant, the cell pellets were resuspended in 20 mM Tris-HCl (pH 8), 400 mM NaCl, and 10 mM imidazole, lysed by sonication, and clarified by ultracentrifugation (100,000 *g* for 45 min). The clarified cell lysate was loaded onto a nickel affinity column (GE Healthcare), which was equilibrated with 20 mM Tris-HCl (pH 8), 400 mM NaCl, and 10 mM imidazole and proteins were eluted using a 0.5 M imidazole gradient. The Vt triple mutant was purified on a GST affinity chromatography column. Octa-histidine and GST affinity tags were removed by overnight cleavage with PreScission protease at 4 °C and dialyzed into 20 mM Tris (pH 8), 400 mM NaCl, 1 mM DTT, and 1 mM EDTA. Proteins were further purified by gel filtration using a Superdex 75 column (GE Healthcare). FRET probes were purified by nickel affinity chromatography and gel filtration using a Superdex 75 column (GE Healthcare), equilibrated in 20 mM Tris-HCl (pH 7.5), 150 mM NaCl, and 0.1 mM EDTA.

MVt/PIP_2 Crystallization

Initially, we used full-length PIP_2 but the crystallization trails of human MVt (residues 959–1134) in complex with PIP_2 were not successful. Next, we used varying concentrations of PIP_2diC_4 ranging from 50 to 500 μM and observed spontaneous nucleation in the Eppendorf tube. Optimizing these seeds or small crystals (less than 10 μm) yielded crystals which diffracted the X-rays from 5 Å to 20 Å Bragg spacings at various beam lines (11-1 at Stanford Synchrotron Radiation Laboratory, SSRL, or 22ID and 22BM at the Advanced Photon Source, APS, of the Argonne National Laboratory, ANL). We improved the crystals by incubating MVt with 100 μM PIP_2diC_8 (Avanti Polar Lipids) on ice for 1 hour and removing the precipitate by centrifugation (15,800 *g* for 30 min at 4 °C). We screened several commercially available crystallization screens (over 1,000 conditions) and obtained a crystallization hit from the PEG/Ion kit of Hampton Research. Crystals grew to 250 μm within 3 days by hanging drop vapor diffusion from

20 mM citric acid, 80 mM Bis-Tris propane (pH 3.4), and 16% (w/v) PEG 3350 at 20 °C that diffracted X-rays at 22ID at APS/ANL to ~3.1 Å Bragg spacings. Crystals were cryoprotected in perfluoropolyether cryo oil and flash frozen and stored in liquid nitrogen at 100 K.

MVt Δ1131-4/PIP_2 Crystallization

Human MVt (residues 959-1130) was incubated with 100 μM PIP_2diC_8 (Avanti Polar Lipids) on ice for 1 hour and the precipitate was removed by centrifugation (15,800 *g* for 30 min at 4 °C). Crystals grew to 250 μm within 3 days by hanging drop vapor diffusion from 20 mM citric acid, 80 mM Bis-Tris propane (pH 3.4), and 12% (w/v) PEG 3350 at 20 °C that diffracted X-rays at 22ID at APS/ANL to ~2.75-Å Bragg spacings. The mother liquor was supplemented with 5% increments of glycerol to 25% and transferred and stored in liquid nitrogen at 100 K.

MVt R975W and MVt R975W/PIP_2 Crystallizations

Human DCM/HCM-associated mutant (R975W; residues 959-1134) crystals grew to 300-400 μm by hanging drop vapor diffusion method from 0.1 M Na-citrate tribasic dihydrate (pH 5.6), 2% Tacsimate (pH 5), and 16% PEG 3350 at 20 °C that diffracted X-rays at BL12-2 at SSRL to ~2.45 Å Bragg spacings. Initial attempts of crystallizing the MVt R975W/PIP_2 complex resulted in heavy precipitation even at PIP_2 concentrations of only 50 μM. Co-crystallization of this complex was eventually achieved with 10 μM PIP_2diC_8. Crystals grew to 300-500 μm within 3 days by hanging drop vapor diffusion from 0.2 M $LiSO_4$, 0.1 M HEPES (pH 7.5), and 22% PEG 3350 at 20 °C and were soaked in 0.5 to 1 mM PIP_2 overnight. These crystals diffracted X-rays at BL12-2 at SSRL to ~2.9 Å Bragg spacings.

MVt Q971R, R975D, T978R Mutant/PIP_2 Crystallization

Human MVt (residues 959-1134) triple mutant protein was incubated with 50 μM PIP_2diC_8 (Avanti Polar Lipids) on ice for 1 hour and the precipitate was removed by centrifugation (15,800 *g* for 30 min at 4 °C). Cylinder shaped crystals grew to 400 μm within 3 days by hanging drop vapor diffusion from 12% PEG 3350, 2% tryptone, and 0.05 M HEPES (pH 7) at 20 °C. These crystals have a similar morphology as the Vt/PIP_2 crystals and were grown in the same conditions and diffracted X-rays at 22ID at APS/ANL to ~3.4 Å Bragg spacings.

Vt R903Q, D907R, R910T Mutant/PIP_2 Crystallization

Human Vt triple mutant was incubated with 20 μM PIP_2diC_8 (Avanti Polar Lipids) on ice for 1 hour and the precipitate was removed by centrifugation (15,800 *g* for 30 min at 4 °C). Crystals grew to 300-400 μm within 5 days by hanging drop vapor diffusion from 0.1 M HEPES sodium (pH 7.5), and 1.5 M Lithium sulfate monohydrate at 20 °C. These crystals diffracted X-rays at BL12-2 at SSRL to ~4 Å Bragg spacings.

MVt R975Q, K979Q, R1107Q, R1128Q Mutant/PIP_2 Crystallization

Human MVt (residues 959-1134) quadruple mutant (R975Q, K979Q, R1107Q, R1128Q) was incubated with 100 μM PIP_2diC_8 on ice for 1 hour and the precipitate was removed by centrifugation (15,800 *g* for 30 min at 4 °C). Crystals grew to 250-300 μm within 3 days by hanging drop vapor diffusion from 20 mM citric acid, 80 mM Bis-Tris propane (pH 8.8), and 14 to 16% (w/v) PEG 3350 at 20 °C that diffracted X-rays at 22BM

at APS/ANL to ~2.76 Å Bragg spacings. The mother liquor was supplemented with 5% increments of glycerol to 25% and transferred and stored in liquid nitrogen at 100 K.

X-ray Data Collection and Processing

X-ray diffraction data were collected at the Advanced Photon Source at Argonne National Laboratory (Argonne, IL) beam lines 22ID and 22BM or Stanford Synchrotron Radiation Lightsource (SSRL) 12-2 and integrated and scaled using XDS and SCALA as implemented in autoPROC (2). Data reduction statistics are provided in **Supplementary Tables I** and **II.**

Structure Determination and Crystallographic Refinement

For all MVt structures, phases were obtained by molecular replacement using the program MOLREP (3) using MVt (Protein Data Bank [PDB] entry 3myi) as the search model. PDB entry 1rke was used as the search model of the mutant Vt/PIP_2 structure. For the PIP_2-bound wild type and Δ1131-4 MVt structures, clear solutions with four molecules in the asymmetric unit were obtained in space group *C* 2 resulting in a calculated volume to mass ratio of 3.35 $Å^3$/Da and 2.48 $Å^3$/Da, corresponding to a solvent content of ~0.633 and 0.503, respectively. For the PIP_2-bound MVt quadruple mutant structure, a clear solution with two molecules in the asymmetric unit was obtained in space group $P\,2_12_12_1$ resulting in a calculated volume to mass ratio of 2.53 $Å^3$/Da, corresponding to a solvent content of ~0.513. For the MVt triple mutant/PIP_2 complex structure, there are 4 molecules in the asymmetric unit in space group $P\,3_2$. Finally, the Vt triple mutant structure has two molecules in the asymmetric unit in space group $P\,3_221$.

For crystallographic refinement, maximum likelihood was performed using autoBUSTER (4) by imposing target restraints using the 2.2 Å MVt structure (PDB entry 3myi) for all MVt structures and 2.35 Å Vt structure (PDB entry1rke) for the Vt triple mutant structure. Except the R975W and R975W/PIP_2 complex crystal structures, all other models were improved by non-crystallographic symmetry restraints through local structure similarity restraints (5). Iterative cycles of model building were performed using Coot (6), and model bias was minimized by building into composite omit maps. Optimized PIP_2 ligand coordinates and ligand restraints were obtained from the Grade web server (grade.globalphasing.org). The electron density maps were sharpened using Coot (6) to ensure the directionality and identity of the α-helices in particular for the structures with moderate resolution. The quality of the final model was assessed using MolProbity (7), which revealed no outliers with >95% of the amino acid residues in the favored region of the Ramachandran plot. Crystallographic refinement statistics are provided in **Supplementary Tables III** and **IV.**

The final MVt/PIP_2 model contains four MVt polypeptide chains and five PIP_2 molecules and the final MVt Δ1131-4/PIP_2 complex comprises four MVt polypeptide chains and three PIP_2 molecules. For the MVt quadruple mutant that was co-crystalized in the presence of PIP_2, there are two polypeptide chains with no visible PIP_2 molecule. The MVt triple mutant/PIP_2 complex contains four MVt polypeptide chains and two PIP_2 molecules in the asymmetric unit. The Vt triple mutant, which was co-crystallized in the presence of PIP_2, has two polypeptide chains with no additional densities for PIP_2 at ~4.0 Å resolution.

Lipid Co-Sedimentation Assay

PIP_2 binding to wild type and mutant MVt were assayed as described previously (8). Briefly, lipid vesicles of phosphatidylcholine (PC) and PIP_2 were prepared in chloroform to have a final composition of 85% PC and 15% PIP_2. The lipid mixture was dried under Argon stream and resuspended in 20 mM Tris (pH 8), 400 mM NaCl, and 3 mM DTT (buffer A). Small unilamellar vesicles were then produced by sonication after incubating the vesicles at 37 °C for 30 min. Samples containing 50 μg of total lipid in 12 μl suspension and 50 μM MVt (wild type or mutant) were incubated at 4 °C for 1 hour followed by centrifugation at 100,000 *g* for 30 min. For full-length wild type and R975W mutant MV, buffer A contained 150 mM NaCl. Proteins were at 15 μM concentration. The supernatant and pellet were separated, and the pellet was washed with buffer A two times and resuspended in 12 μl. The supernatant and pellet samples were analyzed by SDS-PAGE.

F-actin Co-Sedimentation Assay

F-actin co-sedimentation assays of MVt proteins were performed as described for Vt(8). Briefly, F-actin (15 μM) was incubated with MVt (8 μM) for 20 min at room temperature and samples were pelleted at 125,000 x *g* for 15 min at 20 °C. The supernatant and pellet were further analyzed on SDS-PAGE and stained for protein bands with Coomassie Blue.

Fluorescence Resonance Energy Transfer (FRET)

The emission spectra of fluorescently tagged proteins were optimized for CFP-MVt fusion proteins at an excitation wavelength of 414 nm with a 455 nm cutoff filter. The emission maxima at 475 nm were observed for CFP-MVt proteins upon excitation at 414 nm, and the emission maxima at 528 nm were observed for YFP-MVt fusion proteins upon excitation at 475 nm.

FRET measurements were performed in the presence and absence of PIP_2 micelles where 1.5 μM CFP-MVt proteins and 4 μM YFP-MVt proteins were mixed and diluted with 20 mM Tris (pH 7.5) and 150 mM NaCl in a total volume of 100 μl. Next, freshly prepared PIP_2 micelles were added to the CFP- and YFP-MVt fusion proteins in the concentration range of 0 to 200 μM and incubated for 10 min at ambient temperature. At higher concentrations of lipid micelles (>200 μM), the proteins tended to precipitate. The fluorescence emission spectrum was measured with a Spectramax M5 plate reader (Molecular Devices, Sunnyvale, CA) and data were collected from at least three different independent experiments for all the FRET pairs.

Isothermal Titration Calorimetry (ITC)

The binding of PIP_2diC8 to purified MVt proteins were investigated by ITC using a VP-ITC microcalorimeter from MicroCal. All experiments were performed in 20 mM Tris (pH 8) and 300 mM NaCl at 25 °C. The sample cell contained 20 to 30 μM MVt proteins and the syringe held 600 to 750 μM of PIP_2. The heat of dilution of the ligand was subtracted from the data before fitting the curve with the Origin 7.0 software.

Microscale Thermophoresis (MST)

Specific binding of PIP_2diC8 to MV full-length proteins was measured by the MST method (9). Human wild type and DCM/HCM-associated MV mutant R975W proteins were labeled with malemide conjugated cysteine reactive NT-647 red dye. Unlabeled

PIP_2diC8 (2.5 to 5 mM) was titrated into a fixed concentration of labeled proteins (1 μM). Binding reactions were carried out in a buffer containing 20 mM Tris (pH 8) and 200 mM NaCl. Before loading the samples, the reactions were incubated for 10 minutes. Samples were loaded into NT.115 hydrophobic capillaries (Nanotemper Technologies) and the data were measured using Monolith NT.115 pico apparatus (Nanotemper Technologies). The data were recorded at 25 °C using the red LED at 20% (GREEN filter; excitation 515-525 nm, emission 560-585 nm) and IR-Laser power at 60%. Data analyses were performed with NTAnalysis and the Origin 7.0 software.

Cell Culture and Microscopy

Vinculin-null MEFs were provided by Keith Burridge (University of North Carolina, Chapel Hill, NC), originally prepared by Eileen Adamson (Sanford-Burnham Medical Research Institute, La Jolla, CA) (10). *Vinculin*-null cells were cultured in DMEM containing 4.5 g/l glucose (Life Technologies) supplemented with 10% FBS, 100 U/ml penicillin, and 100 μg/ml streptomycin at 37 °C and 5% CO_2 in a humidified incubator.

Vinculin$^{-/-}$ MEFs were transfected with either pCDNA4 vector or FL human MV constructs as an *N*-terminal His_{10}-EGFP fusion, using the Amaxa nucleofector kit for MEFs (Lonza) according to the manufacturer's protocol. Cells expressing MV and its variants tagged with enhanced green fluorescent protein (EGFP) were maintained under selection pressure of 0.5 mg/ml zeocin for 2 weeks and sorted using a FACSAria3 cell sorter (Becton Dickinson, Franklin Lakes, NJ). After recovery, the cells were further cultured in the presence of 0.8 mg/ml zeocin to generate stably expressing populations for 1 week and a second round of sorting was performed to enrich the stably expressing protein populations.

After 24 hours of attachment to fibronectin coated coverslips (Neuvitro corp. USA), *vinculin*$^{-/-}$ MEF cells hosting the pCDNA4 vector and the EGFP-tagged MV constructs were fixed with 4% paraformaldehyde (PFA) solution in PBS for 15 minutes, permeabilized with a mixture of 0.2% Triton X-100 for 1 minute and blocked with 1% bovine serum albumin (BSA) in PBS for 1 hour. Actin filaments were stained with mouse Alexa-633-coupled phalloidin (Thermofisher Scientific). For imaging, the coverslips were mounted on a glass slide using Vectashield DAPI containing mounting medium (Vector Laboratories).

Fluorescence images were collected on confocal laser scanning microscope (LSM 780; Zeiss), controlled by Zen software, using a GaAsP detector. Cells were imaged at room temperature using 40×/1.3 NA Plan-Apochromat oil-immersion objective lens. Excitations of the individual fluorophores in the stained cells were achieved using an argon laser (at 488 nm for EGFP), a HeNe laser (at 633 nm for Alexa Fluor 633), and a solid-state laser (at 405 nm for DAPI). Images were further processed using ImageJ for brightness/contrast adjustments for confocal images.

Wound Healing Assay

Vinculin$^{-/-}$ MEFs and the cells stably expressing full-length wild type or mutant MV were seeded at a density of 0.5×10^6 cells per culture-insert in a 35 mm plate (Ibidi USA Inc). Cells were incubated at 37 °C and 5% CO_2 for 24 hours to achieve confluency. The wound-healing assay was initiated by removing the μ-shaped culture-insert and the culture dish was then gently washed with media to remove any cell debris and replenished with 2 ml of fresh media (DMEM with 10% FBS, 100 U/ml penicillin, and 100 μg/ml streptomycin). Cells were imaged on an EVOS FL cell imaging system (Life Technologies) equipped with a color charge-coupled device image acquisition system

(ICX285AQ; Sony) through software built in to the onboard microprocessor. A 10×/0.25 dry objective lens was used for bright field imaging immediately afterwards in order to represent the zero time point, and the wound healing was monitored every 4 hours and returning plates for incubation after every imaging session. All assays were repeated in triplicate. Each time, images were taken along the wound caused by the insert removal and the positions that were similar in wound distance were used for direct comparison.

SUPPLEMENTARY FIGURES

Supplementary Figure S1

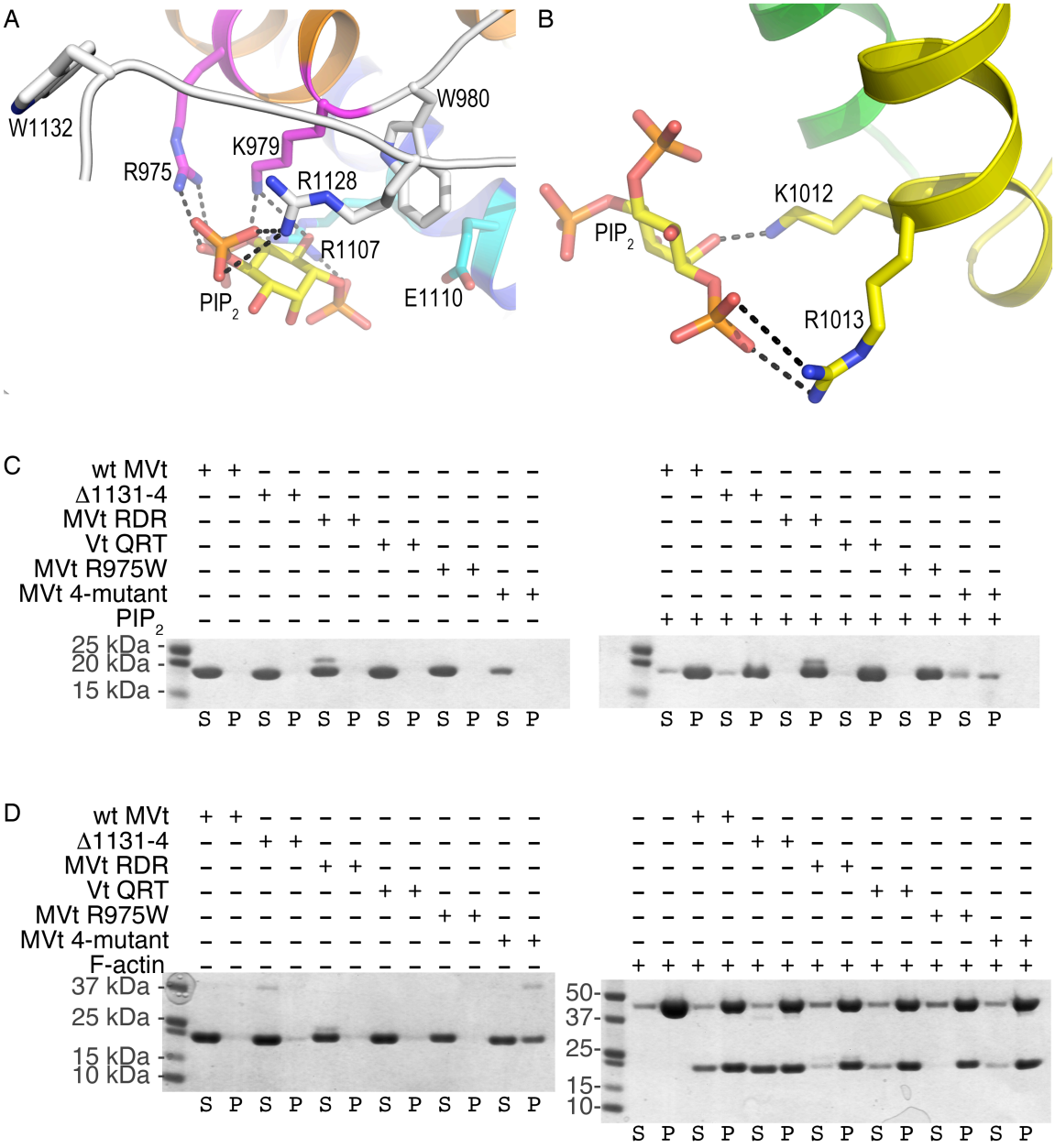

Supplementary Fig. S1. Lipid-induced MV dimerization
A, Close-up view of the PIP_2-binding site as seen in the MVt/PIP_2 crystal structure. R1128 interacts with the PIP_2 4'-phosphate group and R975 and K979 interact with the PIP_2 5'-phosphate group and also interact with the 5'-phosphate group in other subunits in the asymmetric unit. Residues R1107 and E1110 bind the PIP_2 1-phosphate group of the inositol ring.

B, Close-up view of the second PIP_2-binding site. Residue K1012 interacts with the hydroxyl moiety on the inositol head group and R1013 interacts with the 1-phosphate attached to inositol ring of PIP_2.

C, Lipid co-sedimentation assays of various MVt proteins. Unilamellar PC vesicles containing 15% PIP_2 were incubated with wild type MVt, MVt Δ1131-4, MVt Q971R, R975D, T978R (MVt RDR), Vt R903Q, D907R, R910T (Vt QRT), MVt R975W, and MVt R975Q, K979Q, R1107Q, R1128Q (MVt 4-mutant). Since the second PIP_2-binding site formed by K1012 and R1013 is still available, it is not surprising that the proteins still sediment and bind the vesicles. S, supernatant; P, pellet; wt, wild type.

D, Wild type MVt, MVt Δ1131-4, MVt Q971R, R975D, T978R (MVt RDR), Vt R903Q, D907R, R910T (Vt QRT), MVt R975W, and MVt R975Q, K979Q, R1107Q, R1128Q (MVt 4-mutant) were co-sedimented with F-actin and analyzed on Coomassie-stained 4-12% NuPAGE Bis-tris precast polyacrylamide gels. S, supernatant; P, pellet; wt, wild type.

Supplementary Figure S2

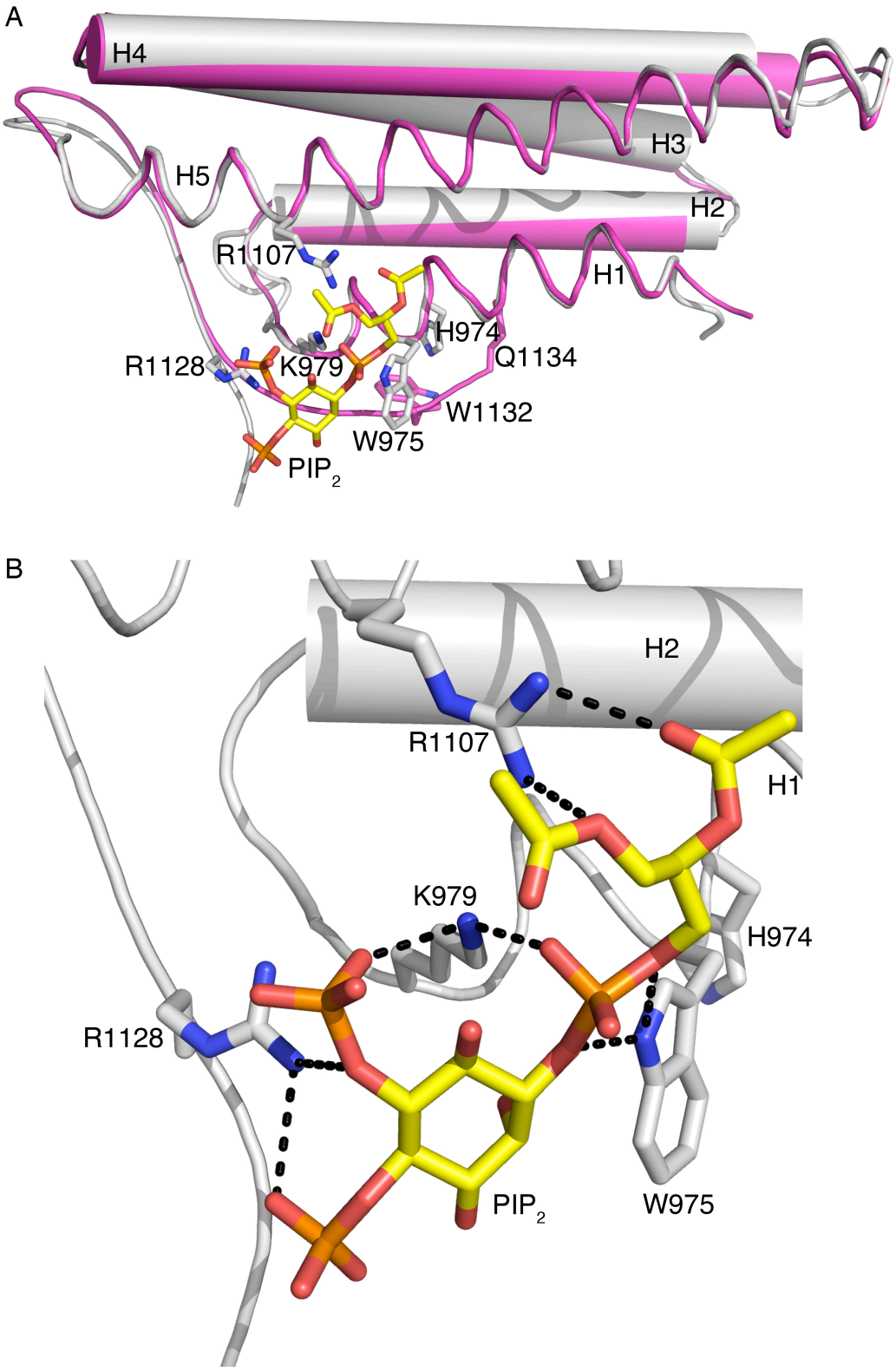

Supplementary Fig. S2. PIP_2 induces the release of the *C* terminus
A, Superposition of the 2.9 Å PIP_2-bound (gray cartoon) and 2.45 Å unbound DCM/HCM-associated R975W mutant (magenta) monomeric structures (*r.m.s.d.* of 0.416 Å for 921 atoms). The PIP_2-unbound R975W mutant MVt structure has its *C* terminus folded back, which is stabilized by an intramolecular cation-π interaction of H974 with W1132. α-Helices are labeled, where H1 and H5 only are shown as ribbons.

B, Close-up view of the PIP_2-binding pocket in the MVt R975W/PIP_2 crystal structure.

Supplementary Figure S3

A

```
      6         7         8         9         0         1         2
959 NQPVNQPILAAAQSLHREATKWSSKGNDIIAAAKRMALLMAEMSRLVRGGSGTKRALIQCAK
891 GEVI---MMM--RQ--D--R--S-K-----------------------------------KR-------

            3         4         5         6         7         8
1021 DIAKASDEVTRLAKEVAKQCTDKRIRTNLLQVCERIPTISTQLKILSTVKATMLGRTNISDE
953  ------------------------------------------------------------

            9         0         1         2         3
1083 ESEQATEMLVHNAQNLMQSVKETVREAEAASIKIRTDAGFTLRWVRKTPWYQ 1134 MVt
1015 ------------------------------------------K------   1066 Vt
```

B

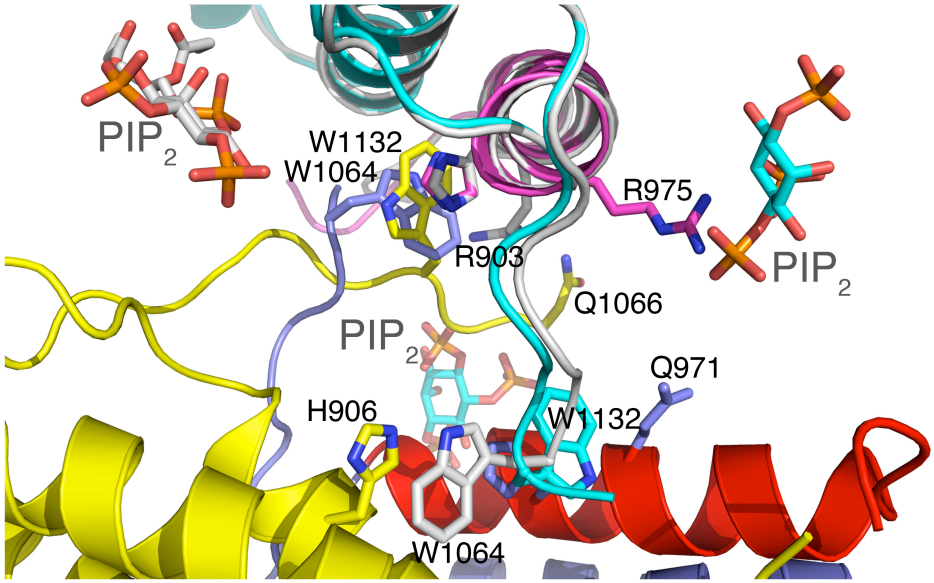

C

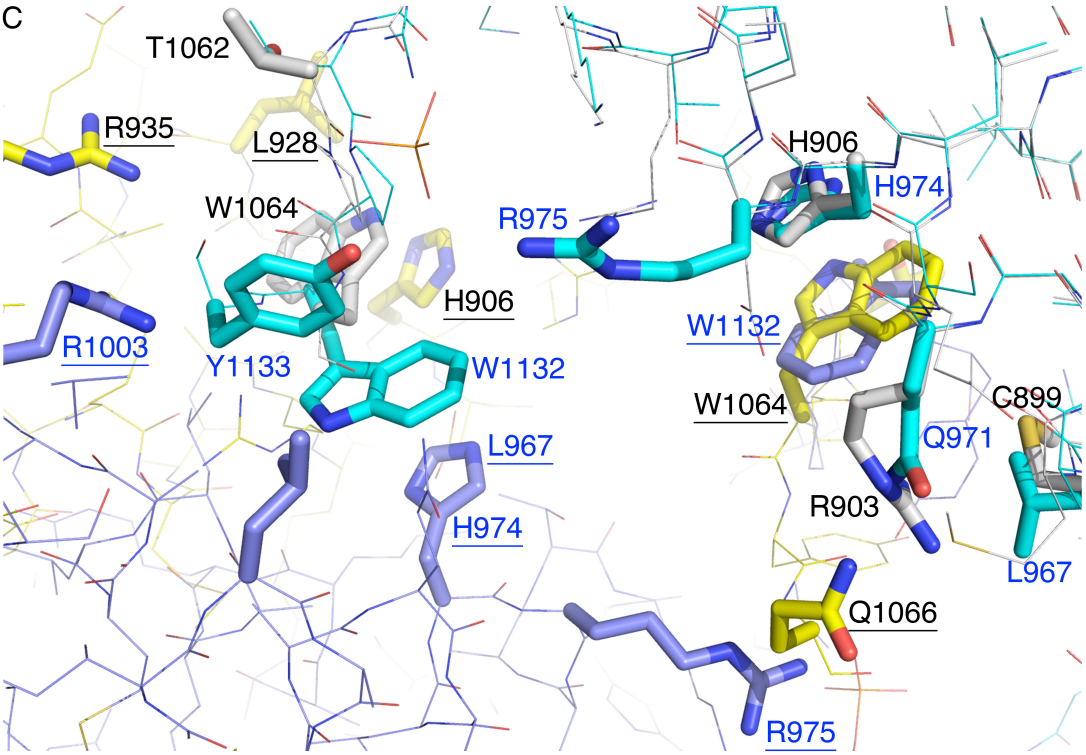

Supplementary Fig. S3. Comparison of MVt and Vt dimers resulting from almost identical building blocks with quasi-equivalent contacts across the interface
A, Structure based MVt (*top*) and Vt (*bottom*) sequence alignment. Residues residing on α-helices are underlined in the MVt sequence. Residues involved in PIP_2-binding are in red font (MVt residues R975, K979, K983, K1012, R1013, R1107, R1128 and Vt residues S913, K915, K944, R945, K1061) and residues involved in intermolecular dimer interactions are highlighted in yellow (MVt residues L967, Q971, H974, L996, A999, R1003, W1132, Y1133, and Vt residues E892, M899, R903, H906, L928, R935, W1064, Y1065). Vt residues 911-1066 and MVt residues 979-1134 are identical which is indicated by a hyphen in the Vt sequence except when the residue is involved in PIP_2-binding. Only the *N* terminus (residues 961-978 in MVt and 893-910 in Vt) that includes the first α-helix (H1' in MVt and H1 in Vt) differs in sequence between the two isoforms.

B, Superposition of one MVt (cyan; H1' α-helix, magenta) onto one Vt (gray) subunit results in similar stacking of W1132 from a second MVt molecule (blue; red for H1' α-helix) and W1064 from a second Vt molecule (yellow) onto their respective histidines (906 in Vt or 974 in MVt). While the Cα of W1064 and W1132 are about 4.6 Å apart, their side chains almost overlap but with opposite orientations. However, since only the MVt protomers within the dimer are related by a 180° two-fold, the respective tryptophan in the second Vt is relatively rotated by almost 180° while still stacking onto its corresponding histidine with a relative Vt to MVt domain movement of about 75°. This allows for the key MVt residue R975 to be in close intermolecular contact with Q971 whereas this quasi-equivalent intermolecular interaction is replaced by R903 and Q1066 in Vt.

C, Close-up view onto the distinct dimer interfaces. The two MVt molecules are shown in cyan and blue, respectively, and key intermolecular interacting residues are labeled in blue and underlined if belonging to the "blue" MVt molecule. The two Vt molecules are shown in gray and yellow and are labeled in black and are underlined if belonging to the "yellow" Vt molecule. The superposition of the "cyan" MVt onto "gray" Vt is shown.

Supplementary Figure S4

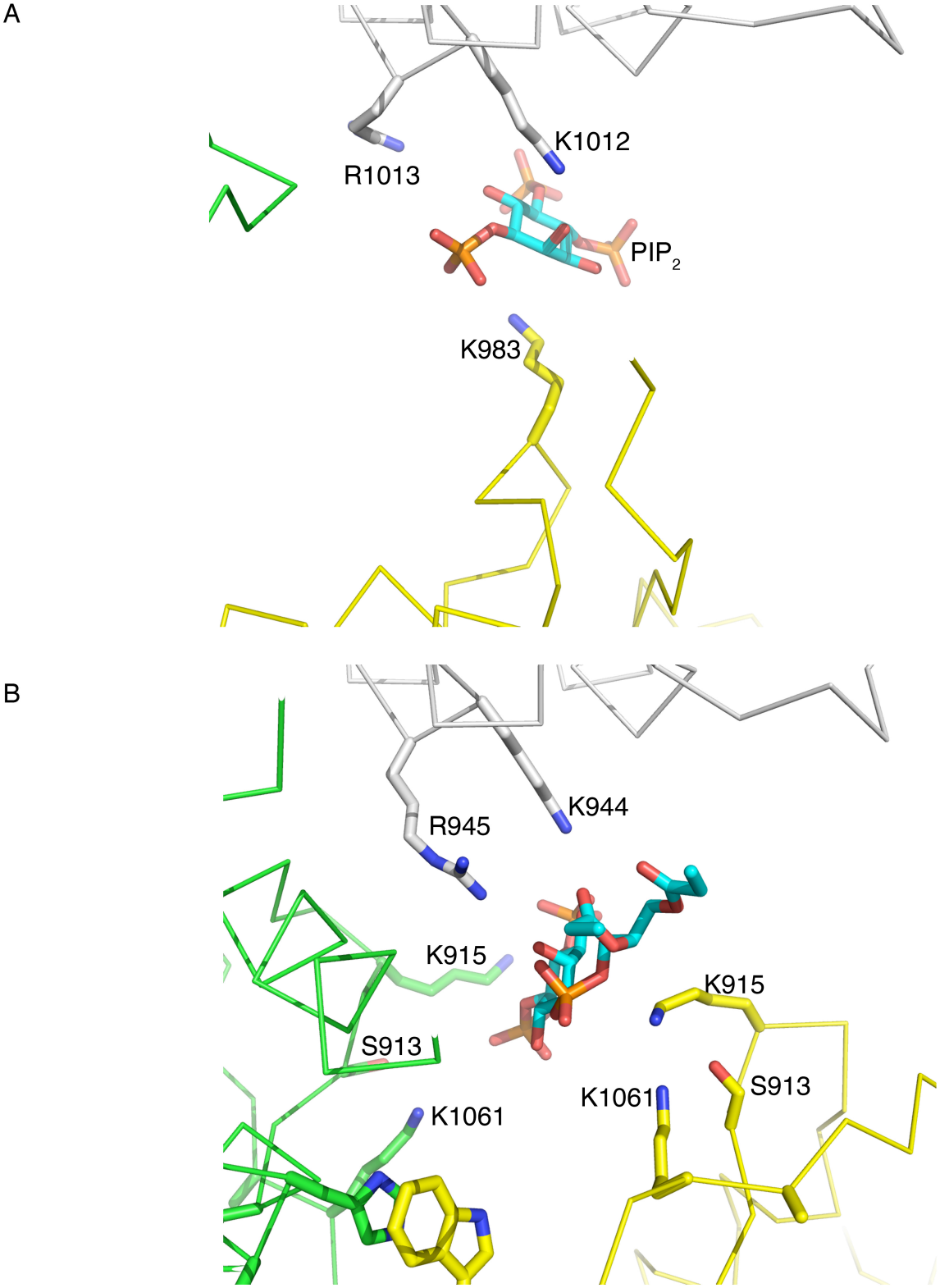

Supplementary Fig. S4. Equivalent and quasi-equivalent interactions define the second lipid-binding site in Vt *versus* MVt

A, Conserved MV residues K1012 and R1013 residing on α-helix H3 (gray cartoon) bind to PIP_2 that is also bound by conserved K983 residing on the H1'-H2 loop region of another MVt (yellow) subunit.

B, Vinculin binding to PIP_2 shown in the same orientation as for MV in panel ***A*** where the equivalent three MV residues bind PIP_2, here K944 and R945 from one subunit (gray) and K915 from two additional subunits (green and yellow, respectively) plus S913 and K1061 from two subunits only seen in the vinculin interaction. While the second PIP_2-binding site is similar in both isoforms, only the PIP_2-bound Vt state allows for binding of three Vt molecules.

Supplementary Figure S5

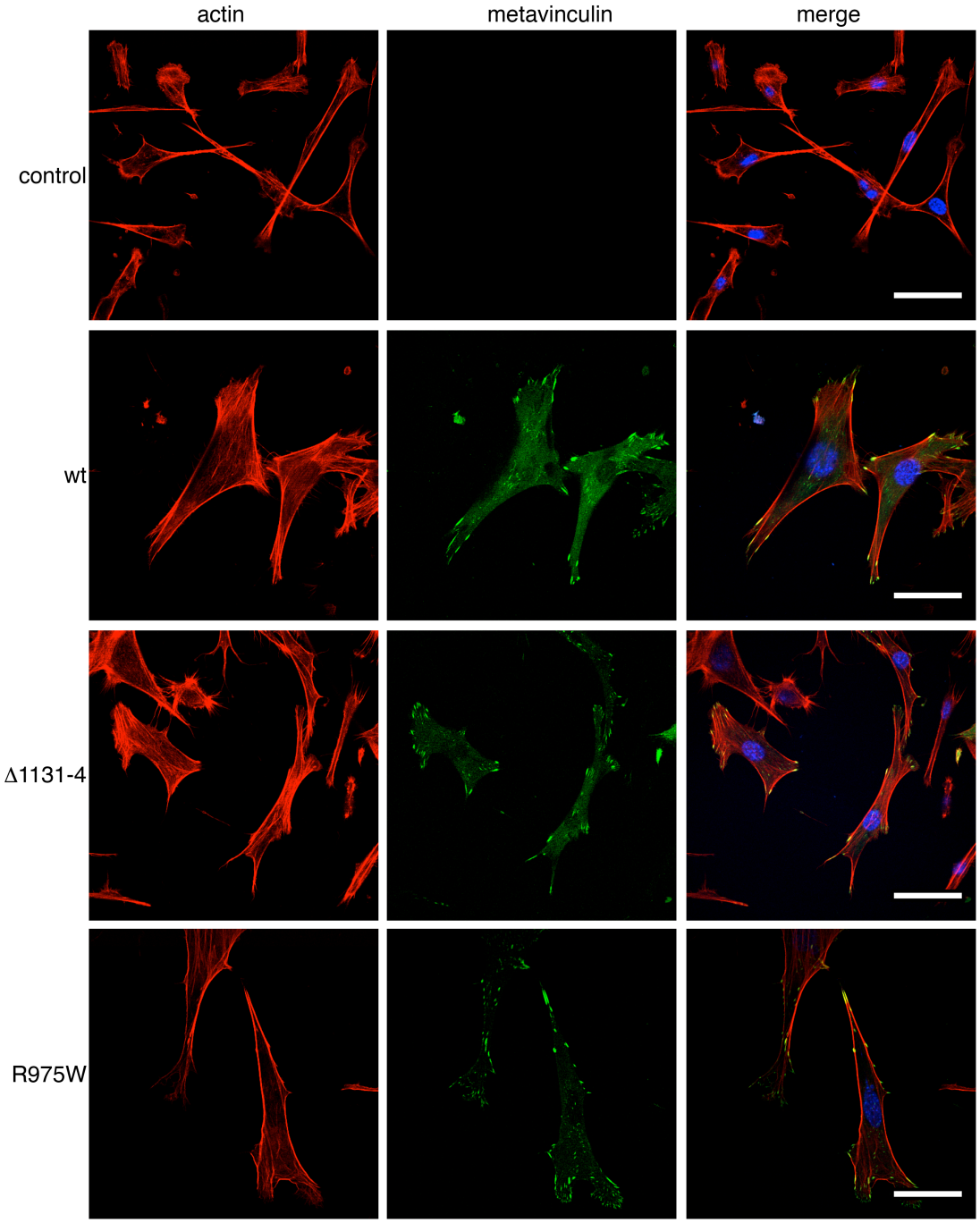

Supplementary Fig. S5. Lipid-directed dimerization of MV contributes to the stabilization of focal adhesions

Vinculin-null MEFs engineered to express wild type GFP-MV (second row) or mutant GFP-MV fusions (R975W or Δ1131-4, third and fourth rows, respectively) were analyzed by confocal laser-scanning microscopy. Representative images, which define the localization of GFP-MV proteins (green, middle panels) at focal adhesions decorating F-actin (red, left panels) and the merged channels were the nuclei are stained with DAPI (right panels), are shown. Scale bars, 50 μm; wt, wild type.

Supplementary Figure S6

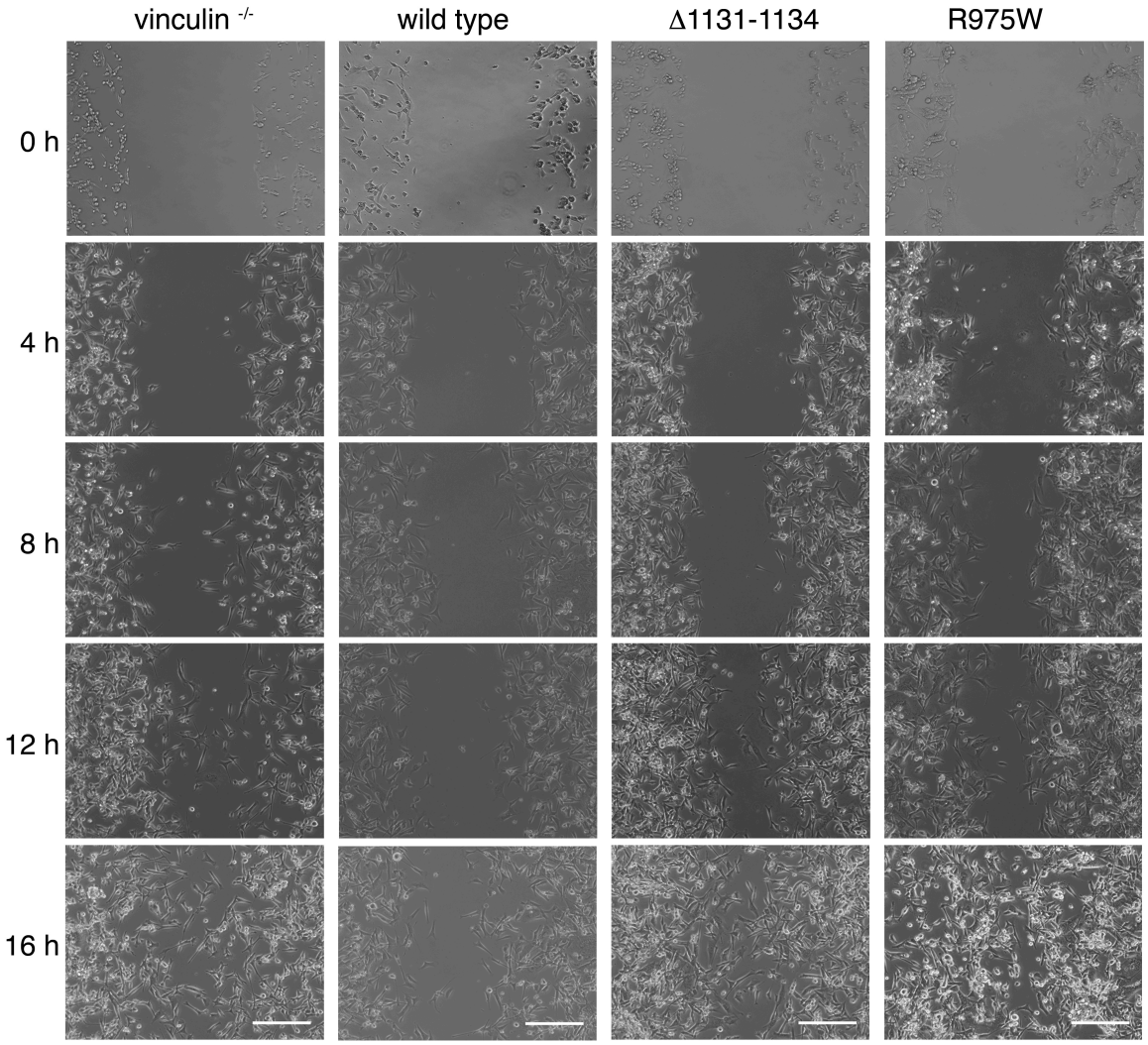

Supplementary Fig. S6. *Vinculin*-null MEFs expressing dimer deficient MV mutants exhibit rapid wound closure

Vinculin-null cells (left panels), the stably expressing human MV (center left panels), and monomeric Δ1131-4 (center right panels) and R975W MV mutants (right panels) on *vinculin*-null cell background were plated onto fibronectin-coated two welled culture-insert containing 35 mm plates as *per* manufacturer's recommendation (0.5 million/ml/well). After 24 hours, the wells were confluent and the monolayers were wounded by removal of the culture-inserts that have a fixed growth area (3.5 cm^2). The extent of cell migration into the wound was recorded initially as 0 hours and subsequent recordings were taken at 4, 8, 12, and 16 hours. *Vinculin*-null cells migrate in a rapid yet chaotic fashion, whereas wound closure in these cells expressing wild type MV is well regulated and an ordered process. *Vinculin*-null cells expressing MV mutant Δ1131-4 showed similar migration to *vinculin*-null MEFs and the R975W mutant MV displayed increased migration and wound closure *versus* cells expressing *vinculin*-null MEFs. The extent of migration for these cells is more rapid than the cells expressing wild type MV. Data shown are representative of four independent experiments. Scale bars, 20 μm.

Supplementary Table I. X-ray data reduction statistics for various (meta)vinculin tail/PIP_2
MVt; MVt Δ1131-4; MVt R975Q, K979Q, R1107Q, R1128Q (MVt 4-mutant); Vt R903Q, D907R, R910T (Vt QRT); and MVt Q971R, R975D, T978R (MVt RDR).

Parameter	**MVt**	**MVt Δ1131-4**	**MVt 4-mutant**	**Vt QRT**	**MVt RDR**
Space group	*C* 2	*C* 2	$P\,2_12_12_1$	$P\,3_221$	$P\,3_2$
Unit cell dimensions					
a [Å]	114.52	120.62	47.15	86.43	56.86
b [Å]	100.68	58.55	70.91	86.43	56.86
c [Å]	105.61	112.49	118.06	175.28	193.13
α	90°	90°	90°	90°	90°
β	122.49°	113.15°	90°	90°	90°
γ	90°	90°	90°	120°	120°
Resolution [Å] overall	89.08 - 3.10	100 - 2.75	60.79 - 2.76	175.2 - 4.00	96.57 - 3.4
Last shell [Å]	3.27 - 3.10	2.90 - 2.75	2.91 - 2.76	4.22 - 4.00	3.73 - 3.4
Total measurements	66,689	166,158	103,164	39,907	107,059
Nr. unique reflections					
Overall	18,132	19,048	10,731	6,727	9,632
Last shell	2,680	2,773	1,517	5,374	2,303
Wavelength	0.97 Å	1.0 Å	1.0 Å	0.9795 Å	1.0 Å
$R_{p.i.m.}$ overall	0.034	0.048	0.022	0.043	0.103
Last shell	0.387	0.071	0.059	0.205	0.266
I/σ(I) overall	15.2	16.3	28.1	13.3	8.5
Last shell	2.1	8.2	13.0	2.9	3.6
Completeness					
Overall	0.982	0.998	0.998	0.987	1.0
Last shell	1.00	0.997	0.997	0.993	1.0
Multiplicity overall	3.7	8.7	9.6	5.9	11.1
Last shell	3.8	8.6	9.1	5.6	11.2
$CC_{1/2}$ overall	0.999	0.995	0.999	0.997	0.983
Last shell	0.742	0.987	0.995	0.896	0.906

Supplementary Table II. X-ray data reduction statistics for DCM/HMC-associated MVt R975W with and without bound PIP_2

Parameter	**MVt R975W/PIP_2**	**MVt R975W**
Space group	*P* $6_4$22	*C* 2
Unit cell dimensions		
a [Å]	80.95	90.07
a [Å]	80.95	41.51
c [Å]	131.76	44.14
α	90°	90°
β	90°	96.13°
γ	120°	90°
Resolution [Å] overall	70.11 - 2.9	44.78 - 2.45
Last shell [Å]	3.08 - 2.9	2.55 - 2.45
Total measurements	250,529	39,167
Nr. unique reflections		
Overall	6,145	5,966
Last shell	946	675
Wavelength	1.0 Å	0.9795 Å
$R_{p.i.m.}$ overall	0.018	0.023
Last shell	0.148	0.024
I/σ(I) overall	43.5	49.2
Last shell	6.8	37.0
Completeness		
Overall	1	0.98
Last shell	1	0.99
Multiplicity overall	40.8	6.6
Last shell	42.5	6.9
$CC_{1/2}$ overall	0.983	0.998
Last shell	0.972	0.998

Supplementary Table III. Crystallographic refinement statistics of various (meta)vinculin tail/PIP_2

MVt; MVt Δ1131-4; MVt R975Q, K979Q, R1107Q, R1128Q (MVt 4-mutant); Vt R903Q, D907R, R910T (Vt QRT); and MVt Q971R, R975D, T978R (MVt RDR) have 4, 4, 2, 2, and 2 MVt polypeptide chains and 5, 3, 0, 0, and 2 PIP_2 molecules in the asymmetric unit, respectively.

Parameter	**MVt**	**MVt Δ1131-4**	**MVt 4-mutant**	**Vt QRT**	**MVt RDR**
PDB entry	5l0c	5l0d	5l0f	5l0j	5l0g
Oligomer	dimer	monomer	monomer	dimer	dimer
Resolution [Å] overall	30.45 - 3.10	50.13 - 2.75	60.79 - 2.76	23.79 - 4.00	49.24 - 3.4
Last shell [Å]	3.29 - 3.10	2.90 - 2.75	3.08 - 2.76	4.47 - 4.00	3.73 - 3.4
No. of reflections (working):	17,144	18,114	10,164	6,335	9,098
No. of reflections (test set):	922	899	526	318	473
R-factor overall	0.2354	0.2067	0.2014	0.2930	0.1797
Last shell	0.2475	0.2244	0.1684	0.3170	0.1973
R-free overall	0.2606	0.2594	0.2417	0.2980	0.2206
Last shell	0.2785	0.2913	0.3036	0.3220	0.2750
No. of non-hydrogen atoms:					
Protein	5,387	5,177	2,739	2,564	5,322
Ligands	140	74	12	0	56
Solvent	61	200	287	16	46
Average B-factor:					
Protein	114.16 $Å^2$	53.06 $Å^2$	26.33 $Å^2$	179.80 $Å^2$	94.91 $Å^2$
Ligands	154.84 $Å^2$	106.45 $Å^2$	59.73 $Å^2$		202.36 $Å^2$
Solvent	79.84$Å^2$	41.26 $Å^2$	35.72 $Å^2$	159.11 $Å^2$	57.75 $Å^2$
R.m.s.d. from ideal values:					
Bond lengths	0.01 Å	0.01 Å	0.01 Å	0.01 Å	0.01 Å
Bond angles	1.13°	1.13°	1.18°	1.8°	1.14°
Ramachandran favored	97.66%	97.72%	99.43%	97.82%	98.81%
Ramachandran allowed	2.34%	2.28%	0.57%	2.18	1.19%
Ramachandran outliers	0	0	0	0	0

Supplementary Table IV. Crystallographic refinement statistics for DCM/HMC-associated MVt R975W with and without bound PIP_2

Unbound and PIP_2-bound MVt R975W have each 1 MVt polypeptide chains and 0 and 1 PIP_2 molecules in the asymmetric unit, respectively.

Parameter	**MVt R975W/PIP_2**	**MVt R975W**
PDB entry	5l0h	5l0i
Oligomer	monomer	monomer
Resolution [Å] overall	70.11 - 2.9	44.78 - 2.45
Last shell [Å]	3.24 - 2.9	2.74 - 2.45
No. of reflections (working):	5,793	5,671
No. of reflections (test set):	323	295
R-factor overall	0.2546	0.1948
Last shell	0.2883	0.2009
R-free overall	0.2778	0.2382
Last shell	0.3780	0.2546
No. of non-hydrogen atoms:		
Protein	1,341	1,363
Ligands	52	7
Solvent	21	65
Average B-factor:		
Protein	90.61 $Å^2$	38.95 $Å^2$
Ligands	165.91 $Å^2$	40.25 $Å^2$
Solvent	78.83 $Å^2$	42.75 $Å^2$
R.m.s.d. from ideal values:		
Bond lengths	0.01 Å	0.01 Å
Bond angles	1.14°	1.1°
Ramachandran favored	99.42%	99.42%
Ramachandran allowed	0.58%	0.58%
Ramachandran outliers	0	0

Supplementary Table V. Thermodynamic parameters for wild type MVt and the DCM/HCM-associated mutant R975W MVt binding to PIP_2 as determined by isothermal titration calorimetry (ITC)

We also performed similar experiments for MVt Δ1131-4 and Vt QRT (R903Q, D907R, R910T) binding to PIP_2 but were unable to saturate the titration and precipitation prevented the determination of binding affinities and stoichiometries.

	K_d	ΔH (kcal/mol)	$T\Delta S$ (kcal/mol)	ΔG (kcal/mol)	N
MVt	0.7 μM	-0.335 ± 0.008	8.05	-8.385	0.483 ± 0.054
	59 μM	-2.328 ± 0.222	3.428	-5.756	0.98 ± 0.81
MVt R975W	2.3 μM	2.178 ± 0.064	9.868	-7.69	0.71 ± 0.015

Supplementary Table VI. Equivalent and quasi-equivalent intermolecular interactions of the lipid-induced MVt and Vt homodimers

A, Equivalent interactions

MVt	Vt
His 974 - Trp 1132	His 906 - Trp 1064

B, Quasi-equivalent interactions

MVt	Vt
Leu 967 - Trp 1132	Leu 928 - Trp 1064
Gln 971 - Arg 975	Arg 903 - Gln 1066
Leu 967 – Trp 1132	Cys 899 – Trp 1064
Arg 1003 – Tyr 1133	Arg 935 – Thr 1062

REFERENCES

1. Rangarajan ES & Izard T (2013) Dimer asymmetry defines α-catenin interactions. *Nat. Struc. Mol. Biol.* 20:188-193.

2. Vonrhein C*, et al.* (2011) Data processing and analysis with the autoPROC toolbox. *Acta Crystallogr. Sect. D. Biol. Crystallogr.* 67:293-302.

3. Vagin A & Teplyakov A (1997) MOLREP: an automated program for molecular replacement. *J Appl Cryst* 30:1022-1025.

4. Bricogne G*, et al.* (2011) BUSTER version 2.9. *Cambridge, United Kingdom: Global Phasing Ltd.*

5. Smart OS*, et al.* (2008) Refinement with local structure similarity restraints (LSSR) enables exploitation of information from related structures and facilitates use of NCS. *Abstr Annu Meet Am Crystallogr Assoc, Knoxville, TN*: abstr. TP139.

6. Emsley P & Cowtan K (2004) Coot: model-building tools for molecular graphics. *Acta Crystallogr. Sect. D. Biol. Crystallogr.* 60(12):2126-2132.

7. Davis IW, Murray LW, Richardson JS, & Richardson DC (2004) MOLPROBITY: structure validation and all-atom contact analysis for nucleic acids and their complexes. *Nucleic Acids Res* 32(Web Server issue):W615-619.

8. Chinthalapudi K*, et al.* (2014) Lipid binding promotes oligomerization and focal adhesion activity of vinculin. *J. Cell Biol.* 207(5):643-656.

9. Duhr S & Braun D (2006) Why molecules move along a temperature gradient. *Proc. Natl. Acad. Sci. U. S. A.* 103(52):19678-19682.

10. Xu W, Baribault H, & Adamson ED (1998) Vinculin knockout results in heart and brain defects during embryonic development. *Development* 125(2):327-337.